



# Depressed mantle discontinuities beneath Iceland: Evidence of a garnet controlled 660 km discontinuity?

J. Jenkins <sup>a,\*</sup>, S. Cottaar <sup>a</sup>, R.S. White <sup>a</sup>, A. Deuss <sup>b</sup>

<sup>a</sup> Bullard Laboratories, Department of Earth Sciences, Madingley Road, Cambridge, CB3 0EZ, UK

<sup>b</sup> Department of Earth Sciences, Universiteit Utrecht, Utrecht, Netherlands



## ARTICLE INFO

### Article history:

Received 18 August 2015

Received in revised form 29 October 2015

Accepted 30 October 2015

Available online 9 November 2015

Editor: P. Shearer

### Keywords:

Iceland  
seismology  
mantle plume  
receiver functions  
transition zone  
mantle discontinuities

## ABSTRACT

The presence of a mantle plume beneath Iceland has long been hypothesised to explain its high volumes of crustal volcanism. Practical constraints in seismic tomography mean that thin, slow velocity anomalies representative of a mantle plume signature are difficult to image. However it is possible to infer the presence of temperature anomalies at depth from the effect they have on phase transitions in surrounding mantle material. Phase changes in the olivine component of mantle rocks are thought to be responsible for global mantle seismic discontinuities at 410 and 660 km depth, though exact depths are dependent on surrounding temperature conditions. This study uses P to S seismic wave conversions at mantle discontinuities to investigate variation in topography allowing inference of temperature anomalies within the transition zone. We employ a large data set from a wide range of seismic stations across the North Atlantic region and a dense network in Iceland, including over 100 stations run by the University of Cambridge. Data are used to create over 6000 receiver functions. These are converted from time to depth including 3D corrections for variations in crustal thickness and upper mantle velocity heterogeneities, and then stacked based on common conversion points. We find that both the 410 and 660 km discontinuities are depressed under Iceland compared to normal depths in the surrounding region. The depression of 30 km observed on the 410 km discontinuity could be artificially deepened by un-modelled slow anomalies in the correcting velocity model. Adding a slow velocity conduit of  $-1.44\%$  reduces the depression to 18 km; in this scenario both the velocity reduction and discontinuity topography reflect a temperature anomaly of 210 K. We find that much larger velocity reductions would be required to remove all depression on the 660 km discontinuity, and therefore correlated discontinuity depressions appear to be a robust feature of the data. While it is not possible to definitively rule out the possibility of uncorrected velocity anomalies causing the observed correlated topography we show that this is unlikely. Instead our preferred interpretation is that the 660 km discontinuity is controlled by a garnet phase transition described by a positive Clapeyron slope, such that depression of the 660 is representative of a hot anomaly at depth.

© 2015 The Authors. Published by Elsevier B.V. This is an open access article under the CC BY license (<http://creativecommons.org/licenses/by/4.0/>).

## 1. Introduction

Iceland straddles the mid-Atlantic Ridge spreading centre between the North American and Eurasian tectonic plates. Its high volumes of crustal volcanism, compared to normal spreading ridges, has lead to the hypothesis of the presence of an underlying mantle plume (e.g. [White and McKenzie, 1989](#)). Geoid anomalies and surface topographic relief as well as petrological and geochemical evidence support this interpretation ([White et al., 1992](#)),

though a minority of authors maintain that a mantle plume is not required to explain the observations ([Foulger and Anderson, 2005](#)).

A major factor in the continuing debate over the presence of an underlying mantle plume is the inability of seismic tomography to reliably identify a plume tail extending through the whole mantle. Seismic tomography constrains anomalies in seismic wave speed which can be due to regional variations in both temperature and composition. Mineral physics predicts that slow seismic anomalies in the mantle are most likely due to high temperatures, so we expect slow seismic wave speeds to be a signature of mantle plumes. While tomographic studies of Iceland all agree on the presence of a strong low-velocity anomaly in the well-resolved upper mantle to depths of several hundred kilometres, deeper structure continues to be ambiguous with much variation between models. To

\* Corresponding author. Tel.: +44 1223337180.  
E-mail address: [jj405@cam.ac.uk](mailto:jj405@cam.ac.uk) (J. Jenkins).

a certain extent this may be due to practical constraints: local studies are severely restricted in depth resolution (down to only ~400 km) due to the small aperture of seismic arrays (Keller et al., 2000), while global models which allow for greater depth resolution only use long period seismic data, resolving long-scale features and missing low-velocity anomalies due to wavefront healing (Montelli et al., 2004). While progression in tomographic methodologies, such as finite frequency and full waveform inversion, have produced more studies reporting hints of plume-tail like structures beneath Iceland (Montelli et al., 2006; Rickers et al., 2013; French and Romanowicz, 2015), tomographic results are still unclear as to the existence of deeper low velocity structure extending through the transition zone.

Even if the continuation of the upper mantle slow velocity anomaly to greater depths beneath Iceland is not currently resolvable tomographically, it is still possible to infer the presence of a temperature anomaly at depth from the effect it has on the phase transitions in the mantle transition zone and the corresponding topography of seismic discontinuities. The transition zone between the upper and lower mantle is delineated by global discontinuities at 410 and 660 km depth. These discontinuities are seen on a global scale, in a range of seismic data types including SS precursors (e.g. Shearer, 1993; Flanagan and Shearer, 1998; Deuss and Woodhouse, 2002; Deuss, 2009), receiver functions (e.g. Lawrence and Shearer, 2006; Andrews and Deuss, 2008), triplications and ScS reverberations (e.g. Revenaugh and Jordan, 1991). They are also observed on smaller regional scales, including several receiver function based studies focused on Iceland (Shen et al., 1996, 1998, 2002; Du et al., 2006).

The transition zone discontinuities are generally interpreted as caused by phase changes in the olivine component of mantle rocks. The olivine to wadsleyite (Ol-Wd) transition causes the 410 km discontinuity (e.g. Katsura and Ito, 1989) and the ringwoodite to perovskite and magnesiowustite transition (Rw-Pv) causes the 660 km discontinuity (e.g. Ito and Takahashi, 1989). The Ol-Wd transition has a positive Clapeyron slope, which means that the 410 km discontinuity deepens in hot regions; the Rw-Pv has a negative Clapeyron slope so the 660 km discontinuity shallows in hot regions (Fig. 1a). The opposite signs of the Clapeyron slopes describing the phase transitions thought to cause the 410 and 660 km discontinuities has led to the classic interpretation of a thickened mantle transition zone (TZ) representing a cold anomaly and a thinned TZ representing a hot anomaly (Fig. 1b and c). Ponding of hot plume material below the 660 km discontinuity, which is predicted based on the negative Clapeyron slope and endothermic nature of the Rw-Pv transition (Hirose, 2002), will lead to further complications, causing uplifted topography on the 660 to be observed across a wider area than the corresponding depression on the 410 (Fig. 1d).

However, olivine is thought to make up only 40–60% of mantle composition, with the remainder predominantly comprising garnet and pyroxenes. Recent studies have highlighted the importance of a phase transition in majorite garnet to perovskite (Mj-Pv) also at 660–700 km, which is thought to become dominant at higher temperatures (Hirose, 2002). Since the Mj-Pv transition has the opposite sign Clapeyron slope to the olivine dominant Rw-Pv transition, in a garnet dominant system a hot anomaly would depress the 660 km discontinuity. This would lead to positively correlated depressed topography on both discontinuities and would have little net effect on the thickness of the TZ (Deuss, 2007), (Fig. 1e).

Most studies consider positive correlation of topography on the 410 and 660 km discontinuities to be due to velocity heterogeneities in the upper mantle, and thus only interpret differential TZ thicknesses. With the improvement of tomographic models, we can correct for upper mantle velocity variations, and interpret absolute discontinuity depths. The mineral physical prediction of a

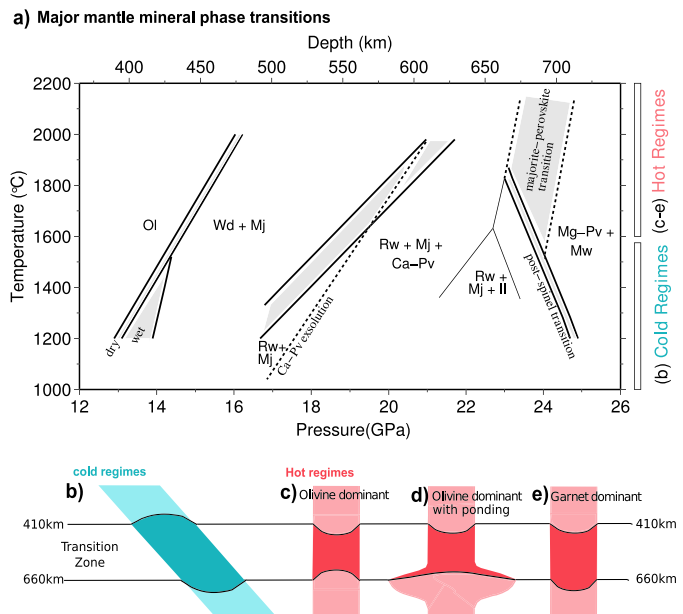


**Fig. 1.** a) Schematic simplified diagram of pressure–temperature dependence of major mantle mineral phase transitions from Deuss et al. (2013) with abbreviations: Ol—olivine, Wd—wadsleyite, Mj—majorite, RW—ringwoodite, Mg-Pv—magnesiowustite (or magnesiowustite), Ca-Pv—calcium perovskite, Il—ilmenite and Mw—magnesiowustite. b–e) Cartoons of predicted discontinuity variation with temperature anomalies adapted from Deuss (2007); b) cold uplifted 410, depressed 660, thickened TZ; c) hot—depressed 410, uplifted 660 and thinned TZ regimes in an olivine dominant system; d) as for c) but with ponding of the plume beneath 660 causing uplift across a wider region; e) hot—depressed 410 and depressed 660 with no overall TZ thinning for a garnet dominant regime and no potential for ponding.

garnet transition at high temperatures also provides an indication that a positive discontinuity correlation is not necessarily an artifact. Mapping of absolute discontinuity depths has the potential to shed light on which phase transition is dominant at the base of the mantle transition zone. With the variation in dominant mineral phase transition at 660 km, observations of the TZ thickness are not necessarily always a reliable indicator of temperature variation. Here we use P to S wave seismic conversions at discontinuities (also called receiver functions), to investigate discontinuity topography beneath Iceland in the light of these new ideas.

## 2. Data and method

### 2.1. Seismic data

Seismic data are sourced from a wide spread of stations across the North Atlantic region and a dense network in Iceland itself (Fig. 2a), with the aim of comparing directly the anomalous plume affected area to surrounding reference regions. Outside Iceland we use data from a total of 37 seismic stations located in Greenland, Jan Mayen, the Faroe Islands, the Shetlands, Scotland, England and Northern Ireland. These publicly available data are accessed through IRIS and ORFEUS data centres from a number of contributing national (Danish—DK, Norwegian—NO/NS, British—GB, N. Irish—EI) and temporary networks (North East Atlantic Tomography—NEAT).

Within Iceland we make use of the IRIS station BORG which has been in operation for over 20 yr, two temporary networks (ICEMELT (Bjarnason et al., 1996), 17 instruments between 1993–1996 and HOTSPOT (Foulger et al., 2000), 28 instruments between 1996–1998), as well as data from 26 broadband stations running for varied periods between 1995–2014 supplied by the Icelandic Meteorological office (IMO-SIL network). In addition, we use data from the University of Cambridge run network, mainly distributed

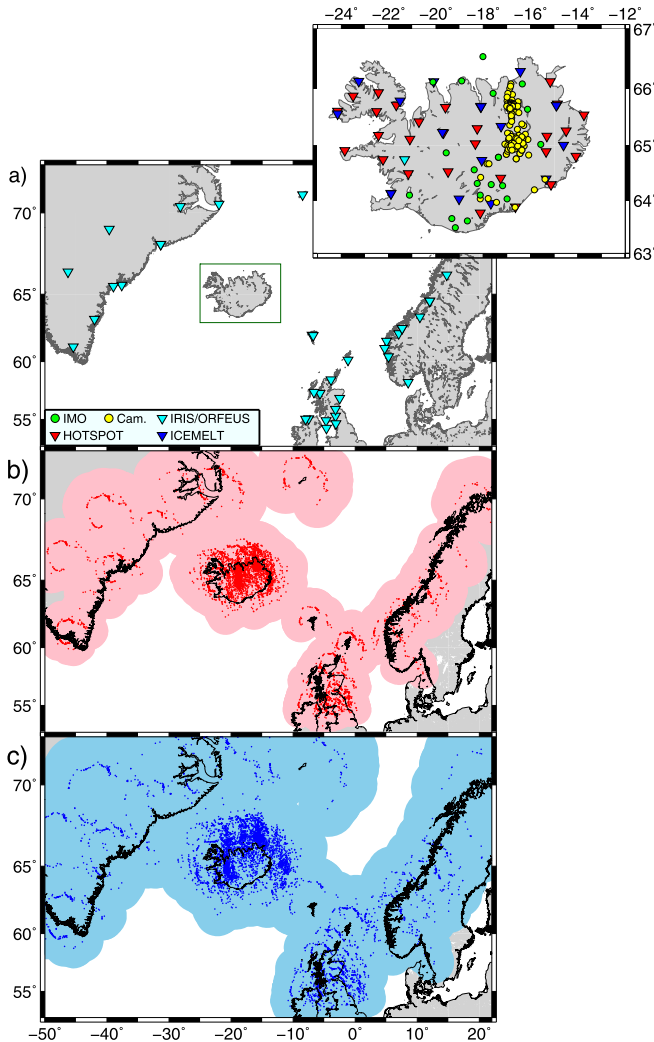


**Fig. 2.** a) Distribution of 37 seismic stations across the North Atlantic and 172 Icelandic stations (inset) used in this study. Pierce points of the 6644 high quality receiver functions in our data set are also shown, plotted as points with their corresponding S-wave Fresnel zone shown by shading at b) 410 km depth and c) 660 km depth.

around the northern volcanic zone, which has been in operation since 2008, giving over 100 further stations, which have been running for varied periods of time over the lifetime of the network.

We select events with magnitude  $M_w$  between 6 and 8.5 occurring during the recording period of the instrument (up to Sept. 2014), at epicentral distances of 30–90°. This distance range is restricted by upper mantle triplications and PP phase interference at <30°, and by diffractions along the core–mantle boundary at >90°. Our final data set contains 1213 events (Fig. 3). Data are band-pass filtered between 0.01–0.2 Hz to reduce interference from local seismicity and remove high frequency noise.

## 2.2. Receiver functions

We use the receiver function technique to image the transition zone discontinuities. When incoming waves from appropriate events interact with mantle discontinuities, some of the direct compressional (P) wave energy is converted to shear (S) wave energy. Such converted waves are referred to as Pds phases, where d denotes conversion depth (e.g. P410s and P660s). Due to the near-vertical incidence of incoming raypaths in our restricted epicentral distance range, the direct P wave is preferentially recorded on the vertical component of motion, while later Pds conversions are

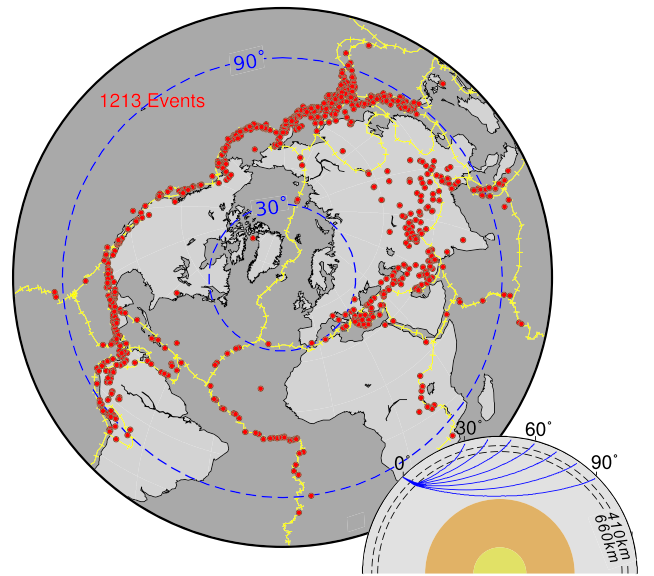


**Fig. 3.** Distribution of the 1213 events in this study (red circles), with blue dashed lines contours at 30° and 90° epicentral distances from central Iceland defining approximate limits of area in which appropriate events fall. Plate tectonic boundaries are shown in yellow cross-hatched lines. Inset—raypaths of P660s phases for epicentral distances between 30–90°.

recorded on the horizontal components. By deconvolving the vertical from the horizontal components we remove the source time function, instrument response and source side effects, producing receiver functions (RFs), which can be interpreted as a direct representation of earth structure beneath the recording station along the incoming raypath (see Fig. 4). We produce RFs via the time domain iterative deconvolution method of [Ligoría and Ammon \(1999\)](#), building the RF with Gaussian pulses of 5 s width. RFs are quality controlled based on reproduction tolerance of >70% (i.e. how well re-convolution of the RF and the vertical component reproduces the horizontal component), signal-to-noise ratio of direct P amplitude to later arrivals and visual inspection. This produces a final data set of 6644 high quality RFs, with 4228 of these sampling the transition zone directly beneath Iceland (Fig. 2b–c).

The RF method assumes that differences in the arrival times between P and Pds phases are due solely to structure along the ray paths above the conversion depth, and that structure in the rest of the mantle is negligible because the P and Pds wave paths are very similar (Fig. 4b–c). Discontinuity depths are converted from the phase arrival travel times by assuming several velocity models for the upper mantle and crust, starting with the 1D radial model PREM ([Dziewonski and Anderson, 1981](#)).

To determine realistic absolute discontinuity depths it is necessary to account for regional variations in the upper mantle velocity and the crustal thickness. These corrections are of particular importance in our study region since low-velocity anomalies of up to –11% are observed under Iceland ([Rickers et al., 2013](#)), and crustal thickness varies from 10 to 42 km ([Darbyshire et al., 2000](#)).

For crustal corrections we use the high resolution Icelandic model of [Darbyshire et al. \(2000\)](#), which is based on a compilation of crustal RF and seismic refraction experiments. For the region lying outside the bounds of the model of [Darbyshire et al. \(2000\)](#), we use CRUST 1.0, a global model of crustal thickness variation described on a 1 by 1° grid ([Laske et al., 2013](#)), see supplementary material Figure S1 for model limits. Upper mantle velocity variation corrections are based on tomographic models. Since we expect strong low-velocity anomalies in the upper mantle beneath Iceland, the choice of correcting model has the potential to severely impact our results. To combat this we perform corrections with three different tomographic models on varying scales: the global

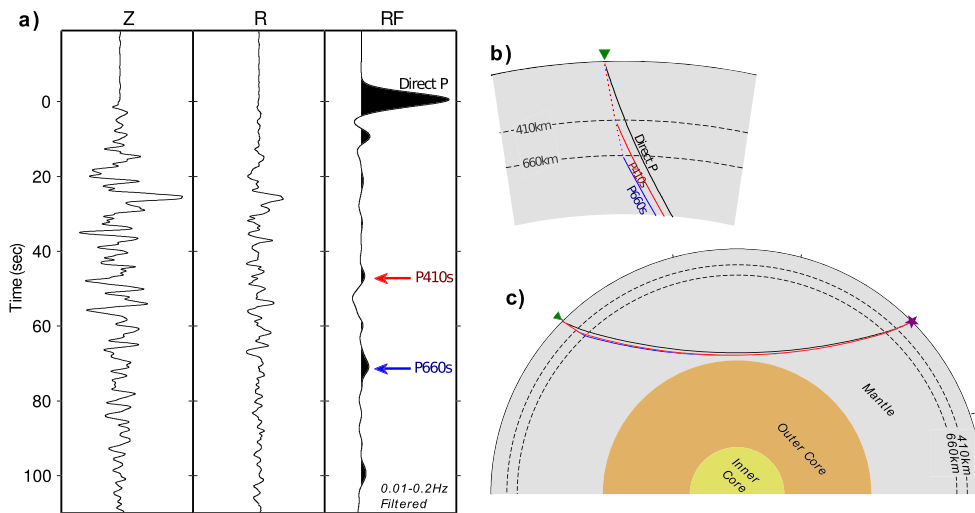


**Fig. 4.** a) Examples of vertical (Z) and radial (R) components of ground motion for an event recorded at IRIS station BORG and the resulting RF obtained by deconvolving the vertical from the radial component. b) Raypaths of direct P (black), P410s (red) and P660s (blue) phases arriving with near-vertical incidence beneath recording station (triangle) which are visible in RFs, where solid lines are P and dashed lines are S raypaths. c) The full raypaths of these phases from source (star) to receiver (triangle), showing high degree of coincidence along the majority of their paths.

model S4ORTS (Ritsema et al., 2011), the continental scale adjoint tomographic model EU60 (Zhu et al., 2015), and the regional adjoint tomographic model of the North Atlantic by Rickers et al. (2013), hereafter referred to as RICK2013 (see supplementary material Figure S2 for visual comparison). S4ORTS and RICK2013 are shear wave velocity models, thus we use a depth dependent scaling factor to calculate P wave velocity variations based on that proposed for S4ORTS (Ritsema et al., 2011), whereas EU60 contains models of both P and S velocity, which are used separately.

### 2.3. Common conversion point stacking

Pds phases are small in amplitude compared to direct P arrivals and are not easily observed above noise level in single RFs. We enhance the Pds arrivals and suppress incoherent noise by stacking RFs with common conversion points (Dueker and Sheehan, 1997; Lekic et al., 2011). A gridded volume is defined from 60°W to 20°E longitude in steps of 0.5°, from 50°N to 75°N latitude in steps of 0.5° and from 50 to 1200 km depth in steps of 1 km. All RFs are ray traced through this volume with the RF amplitude being added to each grid point which falls within the Fresnel zone of the ray. We define the Fresnel zone as all points within a distance of the Fresnel zone half width (FZHW) away from the ray theoretical path:  $FZHW = \sqrt{(\frac{\lambda}{2} + r)^2 - r^2}$ , where  $\lambda$  is the wavelength based on the dominant period of S waves (~11 s) and velocity, at a specific depth  $r$  (Lekic et al., 2011). RF amplitudes are weighted by distance from the centre of the raypath, with a weighting of 1 throughout most of the Fresnel zone before falling off quickly to 0 near the limit of the Fresnel zone (see supplementary material for more details, Figure S3). Due to the high density of sampling beneath Iceland as a result of the large number of closely spaced stations, Icelandic RFs are added over an area of the true S-wave Fresnel zone based on  $\lambda/2$  in the FZHW equation, whereas outside Iceland the Fresnel zone width is increased as we substitute  $\lambda$  into the FZHW equation in order to increase smoothing over this less well sampled region. We also compute a running standard error using the running average of stacked RF amplitude. Finally, each element is normalised by the number of RFs making up the stack; elements containing fewer than 30 summed RFs are masked out. Pds discontinuity peaks are then extracted from the final volume via running averages over depth at each latitude-longitude point:

picked peaks are only deemed to be robust if they are above twice the standard error of the mean.

## 3. Results

### 3.1. Discontinuity topography

We apply the common conversion stacking technique (section 2.3) to our data set of 6644 Pds RFs sampling the Icelandic and surrounding regions. We first present the results where RFs are time to depth converted using the RICK2013 velocity model, chosen for its high resolution and appropriate coverage of the area under investigation.

Figs. 5 and 6, which are visualizations of our 3D RF stack, show a significant depression of both the 410 and 660 km mantle discontinuities beneath Iceland compared to Greenland, Norway and Scotland, with maximum depressions observed beneath central Iceland. Fig. 5 shows east–west cross sections running through our volumetric stack. The northern-most cross section through 71° latitude (Fig. 5a) shows almost flat 410 and 660 km discontinuities. Moving south, depressed 410 and 660 km discontinuities become visible, which are most pronounced through 64.5° latitude when bisecting Iceland (Fig. 5c). South of Iceland at 62.5° latitude, the data coverage decreases, but it is still possible to observe that the strength of the depression is reduced, with discontinuities starting to return to regional background depths (411 and 662 km on average across the region) (Fig. 5d). The lateral extent of the depressed 410 and 660 km discontinuities is most clearly visible in their topography maps (Fig. 6a and b). The depression is limited to the area beneath Iceland across an almost circular region approximately 400–500 km in diameter, with the strongest depression concentrated in the south–west corner of Iceland. Some variation in the transition zone thickness is also observed (Fig. 6c). Though the region of greatest depression in the discontinuities also occurs in the area of the thinnest TZ under Iceland, the thinning is not particularly large when accounting for general variations observed across the surrounding region (Fig. 6c). The majority of observed TZ thicknesses fall within the range of estimates of the global average thickness of 242.0–250.8 km (Lawrence and Shearer, 2006; Andrews and Deuss, 2008). It is noticeable that a ring of thickened TZ occurs around the area of depression: this is particularly clear off the west coast of Iceland and is due to the depression of the 660 km discontinuity affecting a wider region than the 410 km

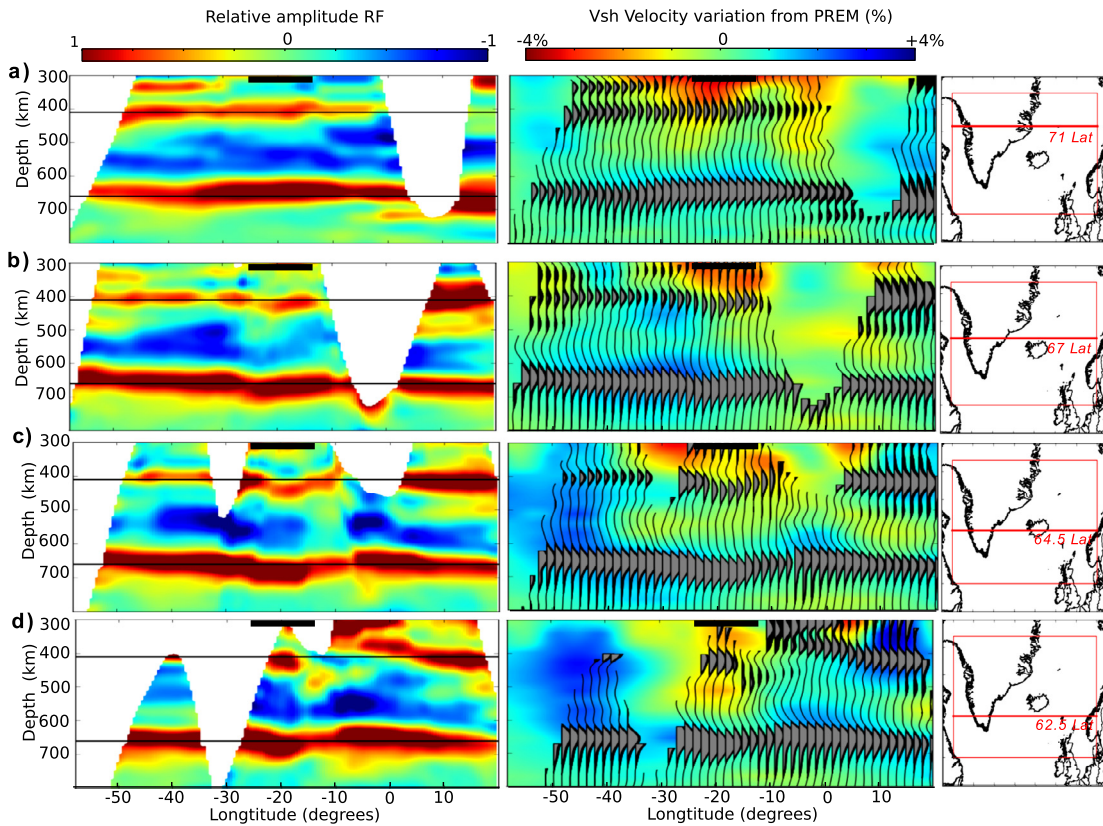


**Fig. 5.** Four east-west cross sections at several latitudes a) 71° b) 67° c) 64.5° d) 62.5°, through our receiver function common conversion stack using the RICK2013 model for depth conversions. Panels on the left show receiver function amplitude with 410 and 660 km depths plotted as black lines. Panels in the centre show RFs plotted as conventional wiggle plots, coloured grey where observations are  $> 2$  standard error, overlain on the shear wave velocity variation from model RICK2013. The location of Iceland is shown as a thick black line at the top of each plot. (For interpretation of the references to color in this figure legend, the reader is referred to the web version of this article.)

discontinuity (diameter of approximately 375 km at the 410 compared to a diameter of 500 km at the 660 km discontinuity).

### 3.2. Influence of the mantle velocity corrections

Our most important observation is a positive correlation of the TZ discontinuities, i.e. both the 410 and 660 km discontinuities are depressed. Positive correlation of TZ discontinuities has generally been disregarded on the assumption that it is an artefact of velocity heterogeneities shallower than 410 km, which affect both phases equally due to the similarity in P660s and P410s raypaths (Shen et al., 1998). However, we observe that even after application of 3D corrections, the positive correlation of the discontinuities appears to be a robust feature of the dataset. Nevertheless, it may be questioned as to whether our observation of depressed 410 and 660 km discontinuities is a consequence of the velocity model chosen for our 3D mantle corrections (RICK 2013), since it will have a large effect on measured discontinuity depths. To investigate this we compare our results to the 1D radial model PREM and two other 3D velocity models: the global shear wave velocity model S40RTS (Ritsema et al., 2011), and the continental compressional and shear wave model EU60 (Zhu et al., 2015).

We find that a depression of both the 410 and 660 km discontinuities is observable independent of the model applied for those tested (Fig. 7). Fig. 7a shows that using a simple 1D PREM velocity model produces unrealistically large depression of the discontinuities. Applying crustal corrections only has a minor influence (Fig. 7b). After application of 3D velocity corrections, the discontinuity depression is dramatically reduced (Fig. 7c-e). All three 3D velocity models produce largely similar discontinuity topography

results, with approximately consistent values of maximum depression on both discontinuities, and with the depression centred in the same location. Additionally we see discontinuity depth values just around the anomalously depressed region that are comparable to values beneath Greenland, Norway and Scotland. These regions are sampled by data from Icelandic stations, giving us confidence that we are accounting sufficiently for the strong near-station velocity variations beneath Iceland. Our tests demonstrate that while it is clearly necessary to account for upper mantle variation and crustal structure to extract realistic discontinuity depths, our results are not strongly biased by our choice of 3D velocity model. The presence of depressed discontinuities independent of the choice of velocity model indicates that this appears to be a robust feature of the data.

## 4. Discussion

We observe a depression of both the 410 and 660 km discontinuities beneath Iceland compared to average depths of 411 and 662 km in the surrounding region, with transition zone thickness close to the global average thickness estimates of 242.0–250.8 km (Lawrence and Shearer, 2006; Andrews and Deuss, 2008). This is consistent with a vertically continuous feature affecting both discontinuities. The fact that the depth anomalies on the 410 and 660 km discontinuities are not anti-correlated indicates that the normal interpretation of an olivine TZ controlled system may not hold true in this setting. Instead, we interpret the depression of both 410 and 660 km discontinuities as indicating a deep sourced mantle plume, assuming that the garnet transition from majorite to perovskite has become dominant at 660 km depth (Fig. 1e).

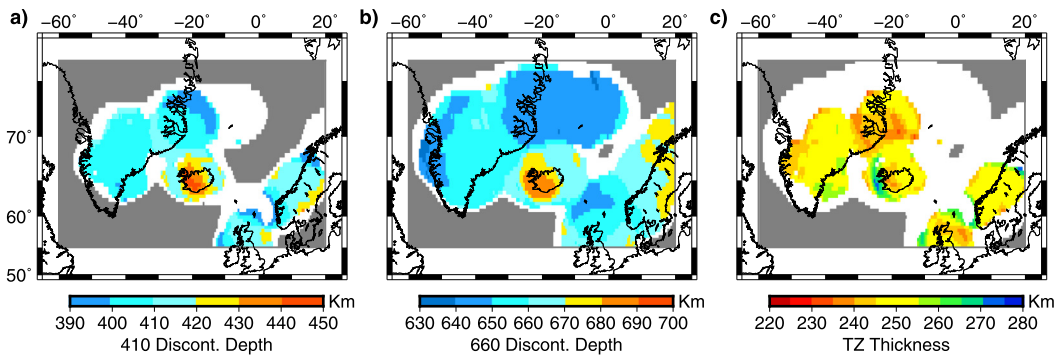


**Fig. 6.** Topography of a) 410 and b) 660 km mantle discontinuities and c) TZ thickness, extracted from the common conversion point stack using the RICK2013 model for depth conversions. Areas of no data coverage are greyed out. White areas show locations where the volume stack contains <30 summed weights of RFs or shows no statistically significant Pds arrival. (For interpretation of the references to color in this figure legend, the reader is referred to the web version of this article.)

The observation of depressed 410 and 660 discontinuities beneath Iceland is not unprecedented, with similar observations made by several previous RF studies (Shen et al., 1996, 1998, 2002; Du et al., 2006; Tauzin et al., 2008). However, positive correlation of TZ discontinuities has, in most earlier studies, been disregarded on the assumption that it is an artefact of velocity heterogeneities shallower than 410 km. Du et al. (2006) comment that this assumption may prove invalid in cases where velocity variations extend through the TZ (such as when considering the scenario of a deep sourced mantle plume), thus affecting only the P660s phases, and negating the justification of interpreting TZ thickness alone. However, by including 3D corrections for crustal thickness and upper mantle velocity variations we attempt to interpret separately the depths of both discontinuities, rather than just differential depth, and show that both are indeed depressed.

Shen et al. (2002) investigate differential arrival times between P410s and P660s phases in RF sampling beneath Iceland, in comparison to predicted differential times from 1D model iasp91. They find smaller than predicted differential arrival times, indicating a thinned TZ, in an anomalous region centred in south central Iceland. In contrast we find the centre of our depressed region and corresponding thinnest TZ in central western Iceland, offset slightly north-west from the centre of the Shen et al. (2002) observation (Fig. 8c). We use the same base data set as Shen et al. (2002) from the temporary networks of HOTSPOT and ICEMELT, but the majority of our data come from the additional stations of the University of Cambridge and Icelandic Meteorological Office networks. The distribution of Cambridge university seismic stations throughout the northern volcanic zone provides higher density RF sampling of central western Iceland at depth, due to the large number of incoming events sourced from central and southern America (Fig. 3). We test the robustness of our results by removing the additional data, reducing our dataset to that available to Shen et al. (2002). In the reduced data set stack, the centre of the depressed region in the 410 topography shifts towards the south-east, moving the maximum thinned TZ centre to a location more similar to that of Shen et al. (2002). Adding our additional data, one station at a time, shows that the updated anomaly location is not biased by a small number of stations, but is required by all new data.

We also note that our location of depressed discontinuities and thinnest TZ in SW Iceland is slightly offset from features seen in tomographic models. The seismically slow anomalies extending through the TZ which are interpreted as a plume tail by Rickers et al. (2013) in their full waveform inversion of the North Atlantic, centre slightly south of the main body of our anomalous region (Fig. 8a and b). Thus our data appear to indicate a slightly more north-westerly location of the plume signal than previously interpreted in other seismic studies.

#### 4.1. Depressed 410 km discontinuity

A depression of the 410 km discontinuity is indicative of a hot temperature anomaly, according to the positive Clapeyron slope of the olivine–wadsleyite transition. Estimates of the Ol-Wd Clapeyron slope have been derived from multiple experimental and first principle calculation studies with most centring on a gradient of approximately 2.5 MPa/K (Ashida et al., 1987; Bina and Helffrich, 1994; Yonggang et al., 2008), though values have ranged from as low as 1.8 MPa/K (Akagi et al., 1989) to as high as 4 MPa/K (Katsura et al., 2004). Taking the maximum observed change in boundary topography under Iceland of approximately 30 km, it is possible to calculate the temperature anomaly required to produce such topography using a chosen Clapeyron slope value. The minimum and maximum Clapeyron slope estimates translate to an excess temperature anomaly ranging from 250 to 555 K. An intermediate value of +3 MPa/K (allowing direct comparison with previous studies), leads to an estimate of 330 K plume anomaly. This is significantly higher than previous estimates of a mantle plume anomaly of 130 K derived from the crustal magmatism generated during continental rifting above the Iceland mantle plume (White and Smith, 2009) and of approximately 200 K for multiple other seismic studies (Rickers et al., 2013; Tauzin et al., 2008; Shen et al., 2002). See Vinnik et al. (2005) for a review of mantle temperature estimates.

Though we consider the Rickers et al. (2013) model used for time-depth conversions to be robust and well-resolved in the upper mantle (from where the majority of the corrections derive), the offset between the location of the maximum low-velocity anomaly in the model, and the observed discontinuity depression, means there is the potential for a small amount of under-correction in the discontinuity time to depth conversions. This could result in artificially deepened estimates of the discontinuity depths. Such a scenario could also become a problem for unobservable narrow low-velocity anomalies not included in the tomographic model. The velocity anomaly in the model of Rickers et al. (2013) directly above the region of maximum depression is  $-0.69\%$  at 400 km depth, which equates to a temperature anomaly of approximately 100 K (based on relationships derived by Xu et al. (2008) for a pyrolytic mantle assuming  $\delta V_s / \delta T = -3.26 \times 10^{-4} \text{ km s}^{-1} \text{ K}^{-1}$  at 400 km). This is significantly lower than the predicted temperature of 330 K derived from Clapeyron slope analysis of the observed discontinuity depression, which does indicate the presence of additional velocity anomalies that are not accounted for in the model. To explore this possibility we implement a simple inversion strategy taking the calculated temperature from the discontinuity depression and increasing the correcting velocity model to reflect this temperature above the region of depression. Increasing the magnitude of velocity corrections leads to a reduced amount of

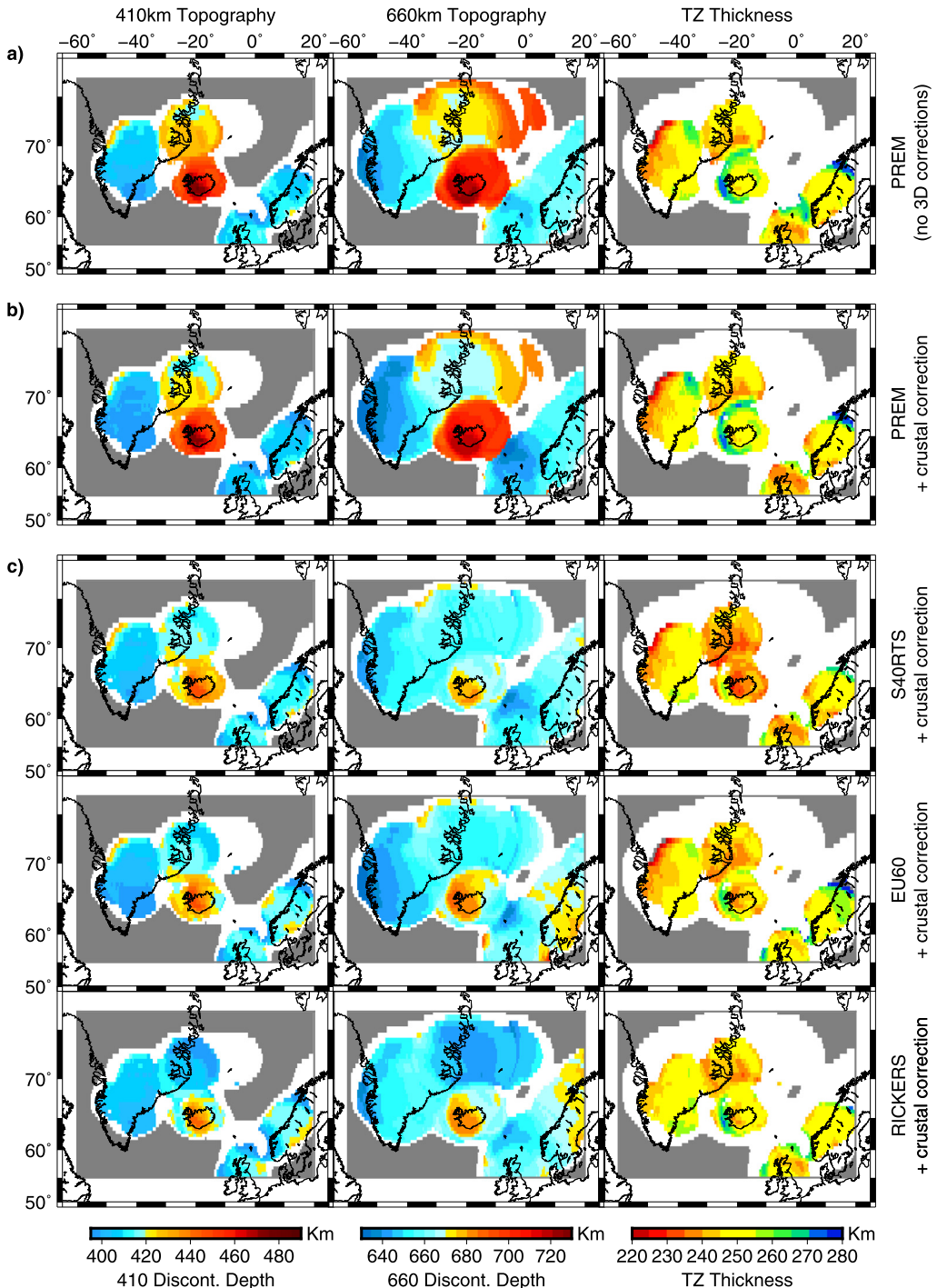


**Fig. 7.** Topography of 410 and 660 km discontinuities and TZ thickness using a variety of different velocity models a) 1D PREM b) PREM plus accounting for variation in crustal thickness combining the model of [Darbyshire et al. \(2000\)](#) and CRUST 1.0 ([Laske et al., 2013](#)), c) Full 3D corrections accounting for variation in crustal thickness and mantle heterogeneity based on the three different tomography models as listed. (For interpretation of the references to color in this figure legend, the reader is referred to the web version of this article.)

observed depression on the discontinuity. From the updated discontinuity depth a new predicted Clapeyron temperature can be calculated and again used to update the velocity model. This process is iterated until we find convergence between the two temperatures, that predicted by the Clapeyron analysis of discontinuity depression and that reflected in the velocity model. This analysis is again preformed assuming a Clapeyron slope of 3 MPa/K. We also assume that shear wave anomalies in the velocity model are due to purely thermal variations, neglecting compositional effects. This means we may slightly overestimate temperature predictions

based on the velocity model, since if there were compositional variations, such as the presence of partial melt in the plume centre, they have the potential to increase the strength of anomalies without representing an increase in temperature.

The results of this experiment suggest that the anomaly within the velocity model needs to be increased to a value of 1.44% from a depth of approximately 280 to 410 km. Both this shear wave speed anomaly and the 19 km of discontinuity depression it produces reflect a temperature anomaly of approximately 210 K, reducing our estimate of temperature anomaly at 410 km by 123 K and bringing

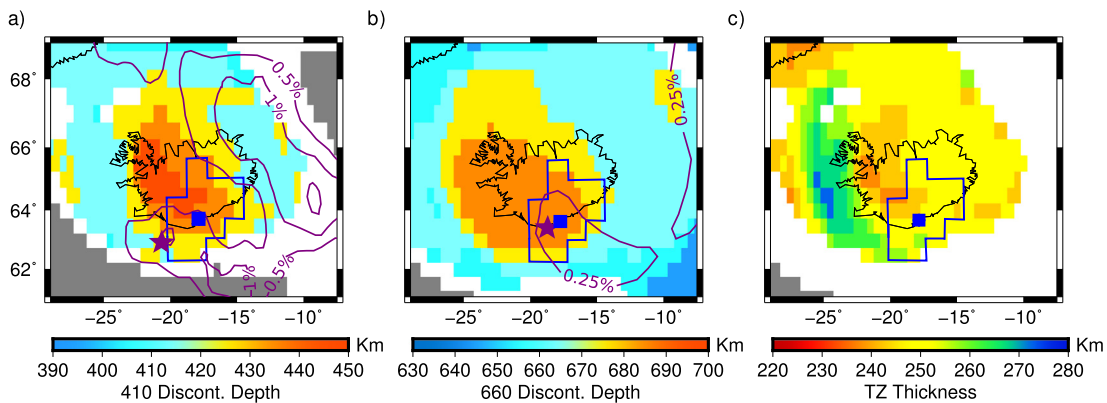


**Fig. 8.** Topography of a) 410, b) 660 km discontinuities and c) TZ thicknesses derived from stacked RF observations, compared to region of anomalously thin TZ identified by Shen et al. (2002) (blue outline with square at interpreted centre), and contoured slow velocity anomalies observed at 400 km and 700 km depth, in the tomographic model of Rickers et al. (2013) (purple outline with interpreted centre shown as a star). (For interpretation of the references to color in this figure legend, the reader is referred to the web version of this article.)

it into a temperature range similar to that estimated in previous studies. Even when this additional velocity anomaly is extended throughout the TZ, thus also affecting the depth of 660 km discontinuity observations, we note that the 660 still appears to be depressed by at least 14 km. Of course all temperature estimates are highly dependent on the choice of Clapeyron slope, which as already discussed can encompass a significant range, so we consider our estimates as only an approximate representation of the true mantle temperatures.

#### 4.2. Depressed 660 km discontinuity—potential causes

A depression of the 660 discontinuity for the ringwoodite–perovskite transition in the olivine mantle component would be indicative of a cold temperature anomaly which, when considering the geological setting and clear indication of a hot anomaly directly above it, is highly unlikely.

A second option is that the velocity model applied underestimates the amplitude of slow velocity anomalies above the TZ, an often-cited reason for interpreting only differential discontinuity depths. However we show that depressed 410 and 660 km discontinuities are visible in our data using three different tomographic models, which in the upper mantle at least are likely to be well resolved. We also performed tests increasing the strength of velocity anomalies in our favoured tomographic model (RICK2013) and find that it can be doubled in strength without removing the depression of the 660 km discontinuity and leading to anti-correlation of the 410 and 660 km discontinuity topography. Thus we consider that the velocity corrections applied adequately correct for upper mantle structure. This is further supported by comparing topography extracted with and without the application of velocity corrections (Fig. 7a and c). Prior to corrections, converting observations from time to depth using only the PREM model, the depression is observed spread across a wide region around Iceland (Fig. 7a). Following corrections, the majority of this depression is removed with only a localised depressed area remaining, while the surrounding region reflects discontinuity depths similar to surrounding regions outside Iceland.

A more pertinent problem is whether any of the velocity models we investigate sufficiently image the velocity structure at greater depths extending through the TZ itself, or are able to fully resolve narrow slow-velocity anomalies caused by a plume conduit, since it is a well known that tomographic models underestimate the amplitudes of velocity anomalies that are smaller than the wavelength of the seismic phases used to construct them (Montelli et al., 2004). Our favoured model RICK2013 shows anomalies extending through the TZ, which the authors interpret

as signs of a plume conduit. However these anomalies are weak (0.5–2%), and though they are visible in similar locations to the depressions we image, they are slightly offset to the south.

We have already shown that the temperature and associated velocity anomaly we predict based on the 410 km topography of an additional 1.44% velocity anomaly can be extended through the TZ without removing depression on the 660 km discontinuity. Now we consider the question of how much additional velocity anomaly (on top of that already applied for RICK 2013) would be necessary to remove all topography on the 660, leaving it flat, similar to the exercise preformed by Du et al. (2006). If we assume that a thin conduit is not resolved below a depth of 200 km we require an additional  $-3.5\%$  velocity anomaly to remove all topography on the 660 km discontinuity, the depth of the 410 depression would also be reduced in this case from a maximum of 20 km to 15 km. However, such slow velocity anomalies would reflect high temperatures extending through the TZ, which would be unlikely not to be reflected in any topography on the 660. Thus we consider how much additional velocity anomaly would be necessary to produce the apparent depths we observe if the 660 is in fact uplifted, as predicted for an olivine controlled ringwoodite–perovskite transition in a hot regime. To do this we assume a Clapeyron slope of  $-2.5 \text{ MPa/K}$  (Ye et al., 2014), and a temperature anomaly similar to that reflected in the topography of the 410 km discontinuity (200 K). In this case we would require an additional  $-4\%$  velocity anomaly in a thin conduit anomaly from 200 km depth through the TZ.

The additional velocity anomalies required to invalidate our observations of depression on the 660 km discontinuity, either causing it to become flat, reflecting no temperature anomaly, or uplifted, reflecting an olivine controlled transition, are significantly larger than the maximum anomaly imaged by the RICK2013 model within the TZ ( $-2\%$ ) in any area. The values are also significantly stronger than the additional velocity anomaly of  $-1.44\%$  required, as suggested by our analysis of the 410 km discontinuity depression discussed in Section 4.1. While such large additional values are not outside the realms of possibility they would be indicative of very strong temperature anomalies, which would produce large amounts of topography on discontinuities on their own account. Even if we accept the possibility that all depressed topography on the 660 km discontinuity is caused by uncorrected velocity structure, this still requires the presence of a hot anomaly extending through the transition zone to at least 660 km depth.

#### 4.3. A garnet controlled 660 km discontinuity?

A physical explanation for a depression on the 660 km discontinuity is that the dominant phase transition is a garnet transi-

tion from majorite to perovskite, described by a positive Clapeyron slope, with the depression indicating a hot temperature anomaly (Yu et al., 2011). First principle calculations suggest this transition is likely to happen over a reasonably broad interval of approximately 35 km (Vitos et al., 2006). However it is still possible for wide gradients to produce observable peaks in RF, as shown in the modelling of synthetic RF by Andrews and Deuss (2008). Especially in hotter regions, the garnet phase transition is thought to become dominant over the olivine ringwoodite–perovskite transition (Hirose, 2002). Thus, although under-estimation of velocity anomalies is still a possible explanation for an observation of correlated discontinuity topography, we argue that it also has the potential be a true feature indicative of a garnet controlled 660 km discontinuity instead.

Several recent global studies of hotspot locations have reached a similar conclusion regarding the importance of a garnet transition in hotspot localities. Deuss (2007) used SS precursor observations beneath 26 hotspot locations, finding that in two-thirds of cases there was evidence for deeper than average 410 km discontinuity depths without corresponding shallow 660 km discontinuity depths. Tauzin et al. (2008) made a global RF study focusing on multiple hotspot locations and found that in general the 410 km discontinuity depth under hotspots is at least 10 km deeper than average, but the TZ is not significantly thinned. The possibility of a garnet controlled 660 km discontinuity highlights the importance of not interpreting TZ thickness alone, but also to consider the absolute topography of TZ discontinuities. In agreement with Deuss (2007), we argue that depression of the 410 km discontinuity is the most reliable global indicator of hot anomalies at depth. The topography of the 660 km discontinuity then serves to provide additional constraints.

The presence of depressed 660 km discontinuity implies a garnet dominant 660 km transition and has the potential to provide constraints on plume temperature as it is predicted that the garnet would become only dominant over olivine at approximately 200–300 K above global average mantle temperature (Hirose, 2002). This estimate provides a lower bound on the plume temperature anomaly and is consistent with our estimates of excess temperatures of approximately 210 K based on the topography of the 410 km discontinuity (see section 4.1). However the exact temperature of the cross-over from an olivine to a Garnet controlled 660 km discontinuity is still poorly constrained due to the variations within experimental and first principle studies as to absolute PT conditions where majoritic garnet is stable (e.g. Yu et al., 2011).

Temperature variation may be expected to increase gradually from background mantle temperatures to the highest temperatures at a plume centre, rather than a step increase. Thus it's possible for the outermost edge of a plume anomaly to show an olivine controlled uplifted 660 km discontinuity before increased temperatures towards the plume centre changes the dominant mineralogy to a garnet controlled depressed 660 km discontinuity. The location of this change would be dependent on the exact temperature at which garnet becomes dominant over olivine. We do not observe a change from uplift to down-warping in our RF stack, which may suggest that such a feature is outside the resolution limits of our observations, based on both the frequencies analysed and the smoothing imposed by adding amplitudes over the width of the ray Fresnel zone. However the fact that we see depression only and no uplift of the 660 km discontinuity suggests that if both uplift and then depression were present radially within the plume, depression (and thus a garnet transition), quickly becomes dominant.

The positive Clapeyron slope of a garnet transition should facilitate plume ascent through the 660 km discontinuity (Hirose, 2002), rather than causing ponding, which has been proposed for

the olivine dominant ringwoodite to perovskite transition due to its negative Clapeyron slope. We observe the anomalous region under Iceland to be affected across a wider area at 660 km than at 410 km, with an associated ring-like structure in the TZ thickness. At first sight, this could be interpreted as plume material ponding under the 660 km discontinuity, but this would be inconsistent with the interpretation of a garnet controlled 660 km discontinuity. It is more likely that this feature is an artefact of the stacking procedure, since RFs are stacked across the Fresnel zone of the incoming ray, which increases as a function of depth, and thus is wider at 660 km than at 410 km depth.

While a garnet dominant 660 km discontinuity provides a possible explanation of the observed depression on the 660 km discontinuity in Iceland, it is not necessarily applicable to all plume settings. Observations of a depressed 410 and uplifted 660 as predicted for a normal olivine dominant system have been reported from other hotspot locations such as Hawaii (Wölbern et al., 2006) and Yellowstone (Schmandt et al., 2012).

## 5. Conclusions

Using a large data set of over 6000 receiver functions combined in common conversion point stacks with recent tomographic models to correct for velocity variations, we image the depths of TZ discontinuities beneath Iceland and the surrounding North Atlantic region. We observe a correlated depression of both the 410 and the 660 km discontinuities under Iceland (thus there is no significant TZ thinning) and average depths of 411 and 662 km across the rest of the imaged region. This observation is independent of the choice of correcting velocity model and appears to be a robust feature of the data.

Correlation of the discontinuity topography is opposite to expectations for olivine phase transitions, which predict anti-correlation for a hot thermal anomaly (i.e. depressed 410 and uplifted 660 km discontinuity). This could represent major underestimation of slow velocity anomalies extending through the TZ due to the inability of correcting tomographic models to fully resolve thin plume-conduit features. Alternatively, we prefer to interpret our observations as indicative of a garnet phase transition controlling topography of the 660 km discontinuity. The phase transition in garnet from majorite to perovskite is described by a positive Clapeyron slope (i.e. depressed 660 km discontinuity in hot regions), and is hypothesised to become dominant over olivine at high temperatures.

A garnet dominated mantle sets a minimum bound of excess temperature in the plume conduit at 200–300 K. This range is consistent with the temperature of 210 K we predict based on the topography of the 410 km discontinuity, which also requires an unseen narrow low-velocity conduit of  $-1.44\%$  not imaged in velocity models. The lack of significant TZ thinning associated with a garnet transition highlights the importance of not considering TZ thickness alone as a reliable indicator of the presence or absence of a mantle plume, as previously discussed by Deuss (2007) and Tauzin et al. (2008). Thus we consider topography of the 410 km discontinuity to be the most robust indicator of temperature anomalies at depth. We also argue that our observations indicate that there is a hotspot anomaly underlying Iceland, which is at least continuous throughout the upper mantle and transition zone.

## Acknowledgements

Seismometers for the Cambridge network in Iceland were borrowed from the Natural Environment Research Council (NERC) SEIS-UK (loans 857 and 968), and funded by research grants from the NERC to R.S.W. (NE/H025006/1). Thanks are also extended to the Icelandic Meteorological office for sharing data that were used

in this study. A.D. and J.J. were funded by the European Research Council under the European Community's Seventh Framework Programme (FP7/2007–2013/ERC grant agreement 204995) and by a Philip Leverhulme Prize and J.J. is also funded by NERC (LBAG/148 Task 5). SC is funded by the Drapers' Company Research Fellowship through Pembroke College, Cambridge, UK. Data was downloaded from IRIS DMC and figures made using GMT (Wessel and Smith, 2001). The authors would like to thank all the PhD students and technicians who aid in the running and maintenance of the University of Cambridge seismic network. Dept. Earth Sciences, Cambridge contribution no ESC.3452.

## Appendix A. Supplementary material

Supplementary material related to this article can be found online at <http://dx.doi.org/10.1016/j.epsl.2015.10.053>.

## References

- Akaogi, M., Ito, E., Navrotsky, A., 1989. Olivine-modified spinel–spinel transitions in the system  $Mg_2SiO_4$ – $Fe_2SiO_4$ : calorimetric measurements, thermochemical calculation, and geophysical application. *J. Geophys. Res.* 94 (15), 671–715.
- Andrews, J., Deuss, A., 2008. Detailed nature of the 660 km region of the mantle from global receiver function data. *J. Geophys. Res., Solid Earth* (1978–2012) 113 (B6).
- Ashida, T., Kume, S., Ito, E., 1987. Thermodynamic aspects of phase boundary among  $\alpha$ -,  $\beta$ -, and  $\gamma$ - $Mg_2SiO_4$ . In: High-Pressure Research in Mineral Physics: A Volume in Honor of Syun-iti Akimoto, pp. 269–274.
- Bina, C.R., Helffrich, G., 1994. Phase transition Clapeyron slopes and transition zone seismic discontinuity topography. *J. Geophys. Res., Solid Earth* (1978–2012) 99 (B8), 15853–15860.
- Bjarnason, I.T., Wolfe, C.J., Solomon, S.C., Gudmundsson, G., 1996. Initial results from the icemelt experiment: body-wave delay times and shear-wave splitting across Iceland. *Geophys. Res. Lett.* 23 (5), 459–462.
- Darbyshire, F.A., White, R.S., Priestley, K.F., 2000. Structure of the crust and uppermost mantle of Iceland from a combined seismic and gravity study. *Earth Planet. Sci. Lett.* 181 (3), 409–428.
- Deuss, A., 2007. Seismic observations of transition-zone discontinuities beneath hotspot locations. *Spec. Pap., Geol. Soc. Am.* 430, 121–136.
- Deuss, A., 2009. Global observations of mantle discontinuities using SS and PP precursors. *Surv. Geophys.* 30 (4–5), 301–326.
- Deuss, A., Woodhouse, J.H., 2002. A systematic search for mantle discontinuities using SS-precursors. *Geophys. Res. Lett.* 29 (8), 90–91.
- Deuss, Arwen, Andrews, Jennifer, Day, Elizabeth, 2013. Seismic observations of mantle discontinuities and their mineralogical and dynamical interpretation. *Phys. Chem. Deep Earth*, 295–323.
- Du, Z., Vinnik, L., Foulger, G., 2006. Evidence from P-to-S mantle converted waves for a flat “660-km” discontinuity beneath Iceland. *Earth Planet. Sci. Lett.* 241 (1), 271–280.
- Dueker, K.G., Sheehan, A.F., 1997. Mantle discontinuity structure from midpoint stacks of converted P to S waves across the Yellowstone hotspot track. *J. Geophys. Res.* 102, 8313–8327.
- Dziewonski, A.M., Anderson, D.L., 1981. Preliminary reference Earth model. *Phys. Earth Planet. Inter.* 25 (4), 297–356.
- Flanagan, M.P., Shearer, P.M., 1998. Global mapping of topography on transition zone velocity discontinuities by stacking SS precursors. *J. Geophys. Res., Solid Earth* (1978–2012) 103 (B2), 2673–2692.
- Foulger, G., Anderson, D.L., 2005. A cool model for the Iceland hotspot. *J. Volcanol. Geotherm. Res.* 141 (1), 1–22.
- Foulger, G., Pritchard, M., Julian, B., Evans, J., Allen, R., Nolet, G., Morgan, W., Bergson, B., Erlendsson, P., Jakobsdottir, S., et al., 2000. The seismic anomaly beneath Iceland extends down to the mantle transition zone and no deeper. *Geophys. J. Int.* 142 (3), F1–F5.
- French, S.W., Romanowicz, B., 2015. Broad plumes rooted at the base of the Earth's mantle beneath major hotspots. *Nature* 525 (7567), 95–99.
- Hirose, K., 2002. Phase transitions in pyrolytic mantle around 670-km depth: implications for upwelling of plumes from the lower mantle. *J. Geophys. Res., Solid Earth* (1978–2012) 107 (B4), ECV-3.
- Ito, E., Takahashi, E., 1989. Postspinel transformations in the system  $Mg_2SiO_4$ – $Fe_2SiO_4$  and some geophysical implications. *J. Geophys. Res., Solid Earth* (1978–2012) 94 (B8), 10637–10646.
- Katsura, T., Ito, E., 1989. The system  $Mg_2SiO_4$ – $Fe_2SiO_4$  at high pressures and temperatures: precise determination of stabilities of olivine, modified spinel, and spinel. *J. Geophys. Res., Solid Earth* (1978–2012) 94 (B11), 15663–15670.
- Katsura, T., Yamada, H., Nishikawa, O., Song, M., Kubo, A., Shinmei, T., Yokoshi, S., Aizawa, Y., Yoshino, T., Walter, M.J., et al., 2004. Olivine–wadsleyite transition in the system  $(Mg, Fe) 2SiO_4$ . *J. Geophys. Res., Solid Earth* (1978–2012) 109 (B2).
- Keller, W.R., Anderson, D.L., Clayton, R.W., 2000. Resolution of tomographic models of the mantle beneath Iceland. *Geophys. Res. Lett.* 27 (24), 3993–3996.
- Laske, Gabi, Masters, Guy, Ma, Zhitu, Pasquano, Mike, 2013. Update on CRUST1.0 – a 1-degree global model of Earth's crust. *Geophys. Res. Abstr.* 15 (Abstract EGU2013-2658).
- Lawrence, J.F., Shearer, P.M., 2006. A global study of transition zone thickness using receiver functions. *J. Geophys. Res., Solid Earth* (1978–2012) 111 (B6).
- Lekic, V., French, S.W., Fischer, K.M., 2011. Lithospheric thinning beneath rifted regions of Southern California. *Science* 334 (6057), 783–787.
- Ligorria, J.P., Ammon, C.J., 1999. Iterative deconvolution and receiver-function estimation. *Bull. Seismol. Soc. Am.* 89 (5), 1395–1400.
- Montelli, R., Nolet, G., Dahlen, F., Masters, G., 2006. A catalogue of deep mantle plumes: new results from finite-frequency tomography. *Geochem. Geophys. Geosyst.* 7 (11).
- Montelli, R., Nolet, G., Dahlen, F., Masters, G., Engdahl, E.R., Hung, S.-H., 2004. Finite-frequency tomography reveals a variety of plumes in the mantle. *Science* 303 (5656), 338–343.
- Revenaugh, J., Jordan, T.H., 1991. Mantle layering from ScS reverberations: 3. The upper mantle. *J. Geophys. Res., Solid Earth* (1978–2012) 96 (B12), 19781–19810.
- Rickers, F., Fichtner, A., Trampert, J., 2013. The Iceland–Jan Mayen plume system and its impact on mantle dynamics in the North Atlantic region: evidence from full-waveform inversion. *Earth Planet. Sci. Lett.* 367, 39–51.
- Ritsema, J., Deuss, A., Van Heijst, H., Woodhouse, J., 2011. S4ORTS: a degree-40 shear-velocity model for the mantle from new Rayleigh wave dispersion, teleseismic traveltimes and normal-mode splitting function measurements. *Geophys. J. Int.* 184 (3), 1223–1236.
- Schmandt, B., Dueker, K., Humphreys, E., Hansen, S., 2012. Hot mantle upwelling across the 660 beneath Yellowstone. *Earth Planet. Sci. Lett.* 331, 224–236.
- Shearer, P.M., 1993. Global mapping of upper mantle reflectors from long-period SS precursors. *Geophys. J. Int.* 115 (3), 878–904.
- Shen, Y., Solomon, S.C., Bjarnason, I.T., Nolet, G., Morgan, W.J., Allen, R.M., Vogfjord, K., Jakobsdottir, S., Stefansson, R., Julian, B., et al., 2002. Seismic evidence for a tilted mantle plume and north-south mantle flow beneath Iceland. *Earth Planet. Sci. Lett.* 197 (3), 261–272.
- Shen, Y., Solomon, S.C., Bjarnason, I.T., Purdy, G., 1996. Hot mantle transition zone beneath Iceland and the adjacent Mid-Atlantic Ridge inferred from P-to-S conversions at the 410- and 660-km discontinuities. *Geophys. Res. Lett.* 23 (24), 3527–3530.
- Shen, Y., Solomon, S.C., Bjarnason, I.T., Wolfe, C.J., 1998. Seismic evidence for a lower-mantle origin of the Iceland plume. *Nature* 395 (6697), 62–65.
- Tauzin, B., Debayle, E., Wittlinger, G., 2008. The mantle transition zone as seen by global Pds phases: no clear evidence for a thin transition zone beneath hotspots. *J. Geophys. Res., Solid Earth* (1978–2012) 113 (B8).
- Vinnik, L., Foulger, G., Du, Z., 2005. Seismic boundaries in the mantle beneath Iceland: a new constraint on temperature. *Geophys. J. Int.* 160 (2), 533–538.
- Vitos, L., Magyari-Köpe, B., Ahuja, R., Kollár, J., Grimvall, G., Johansson, B., 2006. Phase transformations between garnet and perovskite phases in the Earth's mantle: a theoretical study. *Phys. Earth Planet. Inter.* 1 (156), 108–116.
- Wessel, P., Smith, W.H., 2001. The generic mapping tools.
- White, R., McKenzie, D., 1989. Magmatism at rift zones: the generation of volcanic continental margins and flood basalts. *J. Geophys. Res., Solid Earth* (1978–2012) 94 (B6), 7685–7729.
- White, R.S., McKenzie, D., O'Nions, R.K., 1992. Oceanic crustal thickness from seismic measurements and rare earth element inversions. *J. Geophys. Res., Solid Earth* (1978–2012) 97 (B13), 19683–19715.
- White, R.S., Smith, L.K., 2009. Crustal structure of the Hatton and the conjugate east Greenland rifted volcanic continental margins, NE Atlantic. *J. Geophys. Res., Solid Earth* (1978–2012) 114 (B2).
- Wölbren, I., Jacob, A., Blake, T., Kind, R., Li, X., Yuan, X., Duennebier, F., Weber, M., 2006. Deep origin of the Hawaiian tilted plume conduit derived from receiver functions. *Geophys. J. Int.* 166 (2), 767–781.
- Xu, W., Lithgow-Bertelloni, C., Stixrude, L., Ritsema, J., 2008. The effect of bulk composition and temperature on mantle seismic structure. *Earth Planet. Sci. Lett.* 275 (1), 70–79.
- Ye, Y., Gu, C., Shim, S.-H., Meng, Y., Prakapenka, V., 2014. The postspinel boundary in pyrolytic compositions determined in the laser-heated diamond anvil cell. *Geophys. Res. Lett.* 41 (11), 3833–3841.
- Yonggang, G.Y., Wu, Z., Wentzcovitch, R.M., 2008.  $\alpha$ – $\beta$ – $\gamma$  transformations in  $Mg_2SiO_4$  in Earth's transition zone. *Earth Planet. Sci. Lett.* 273 (1), 115–122.
- Yu, Y.G., Wentzcovitch, R.M., Vinograd, V.L., Angel, R.J., 2011. Thermodynamic properties of  $MgSiO_3$  majorite and phase transitions near 660 km depth in  $MgSiO_3$  and  $Mg_2SiO_4$ : a first principles study. *J. Geophys. Res., Solid Earth* (1978–2012) 116 (B2).
- Zhu, H., Bozdag, E., Tromp, J., 2015. Seismic structure of the European upper mantle based on adjoint tomography. *Geophys. J. Int.* 201 (1), 18–52.